JCB Journal of Cell Biology

REPORT

# Independent anterograde transport and retrograde cotransport of domain components of myelinated axons

Yoko Bekku and James L. Salzer

**Neurons are highly polarized cells organized into functionally and molecularly distinct domains. A key question is whether the multiprotein complexes that comprise these domains are preassembled, transported, and inserted as a complex or whether their components are transported independently and assemble locally. Here, we have dynamically imaged, in pairwise combinations, the vesicular transport of fluorescently tagged components of the nodes of Ranvier and other myelinated axonal domains in sensory neurons cultured alone or together with Schwann cells at the onset of myelination. In general, most proteins are transported independently in the anterograde direction. In contrast, there is substantial cotransport of proteins from distinct domains in the retrograde direction likely due to coendocytosis along the axon. Early myelination did not substantially change these patterns of transport, although it increased the overall numbers of axonal transport vesicles. Our results indicate domain components are transported in separate vesicles for local assembly, not as preformed complexes, and implicate endocytosis along axons as a mechanism of clearance.**

## Introduction

The exquisite, polarized organization of neurons underlies their function in afferent and efferent reception and propagation of action potentials. A particularly striking example is the organization of myelinated axons, which consists of a series of functionally and biochemically distinct subdomains (i.e., the nodes, paranodes, juxtaparanodes, and internodes; Salzer et al., 2008; Susuki and Rasband, 2008). This organization, which is centered around the nodes of Ranvier, is essential for effective saltatory conduction.

These axonal domains are comprised of distinct sets of transmembrane and cytoskeletal proteins. Nodes of Ranvier, which correspond to just 0.1% of the axon surface, are enriched in a multimeric complex of voltage-gated $Na^+$ channels (NaV) and their associated β subunits, the neuronal cell adhesion molecules (CAMs) neurofascin (NF) 186 and NrCAM; each of these proteins is linked to the cytoskeletal protein ankyrin-G (AnkG) and thereby to the spectrin/actin cytoskeleton. Nodes are flanked by the paranodes, which are the sites of a specialized axon–glial junction formed by a cis-complex of Caspr and contactin linked to the 4.1B cytoskeleton. On either side and just under the compact myelin sheath are the juxtaparanodes, which consist of a complex of Caspr2, TAG1, and the voltage-gated $K^+$ channels, Kv1.1 and 1.2. Finally, the largest domain by far is the internode, corresponding to ∼99% of the axon surface and enriched in the Necl adhesion molecules, which are also linked to 4.1B.

The extent to which these various proteins segregate into separate transport vesicles at the TGN or are cosegregated as preassembled complexes for subsequent targeting and fusion to specific axonal domains is not known (Bentley and Banker, 2016). Prior to myelination, axonal adhesion molecules, as well as ion channels, are diffusely distributed along the axon. With myelination, adhesion molecules concentrate at distinct domains driven in part by interactions with their cognate ligands on the apposed membranes of myelinating glia (Rasband and Peles, 2016). These results suggest that glial interactions recruit adhesion molecules on the axon that pioneer domain assembly. In agreement, we demonstrated that preexisting pools of CAMs that are initially diffusely present on the axon surface redistribute to nucleate domains (Zhang et al., 2012). Thus, NF186 and likely adhesion molecules in other domains are "diffusion trapped" by cognate ligands of Schwann cells (Zhang et al., 2012). In contrast, ion channels and AnkG require transport to peripheral nervous system (PNS) nodes during myelination. These

Neuroscience Institute, New York University Langone Medical Center, New York, NY.

Correspondence to Yoko Bekku: yoko.bekku@nyulangone.org; James L. Salzer: james.salzer@nyulangone.org.

results agree with earlier studies indicating PNS nodes assemble sequentially pioneered by NF186, with the subsequent recruitment of AnkG and $Na_v$ (Dzhashiashvili et al., 2007; Lambert et al., 1997).

Thus, multiple sources of proteins contribute to domain assembly: preexisting proteins on the axon surface, which redistribute, and newly synthesized proteins, which are delivered by anterograde transport. These results suggest that components of the node may be transported independently to axons before myelination and later assembled locally. Of interest, the slow replenishment of all components during maintenance of mature nodes requires transport (Zhang et al., 2012). These latter results raise the possibility that with myelination, node components potentially may be preassembled in the TGN for cotransport and subsequent domain-specific membrane insertion. Evidence of preassembly of complexes has been shown for components of the presynaptic active zone, which exit the TGN as part of a common vesicle (Maas et al., 2012).

Here, we examined directly the axonal transport of distinct transmembrane proteins that are enriched at nodes and other domains in dorsal root ganglion (DRG) neurons cultured alone or with Schwann cells at the onset of myelination. These include CAMs, KCNQ3/Kv7.3, and β subunits of the sodium channel. We found these axonal membrane proteins are largely transported anterogradely in separate vesicles except for NrCAM and NF186, which are cotransported in the same vesicles. In contrast, there is significant cotransport of retrogradely transported proteins that results from endolysosomal clearance. Initial myelination did not alter these patterns of transport but did increase the numbers of transport vesicles in axons. Cotransport of NF186 and NrCAM is mediated by their cytoplasmic segments and depends in part on interactions with AnkG. Taken together, these results strongly suggest that many anterogradely transported vesicles preferentially contain single cargoes rather than preformed domain complexes and are transported to the axon for local assembly.

## Results and discussion

### Domain components are transported separately in the anterograde direction

To assess transport of proteins, we imaged fluorescently tagged proteins expressed in cultures of sensory neurons (schematic shown in Fig. S1 A). We compared transport of NF186, a key component that pioneers PNS nodes of Ranvier (Sherman et al., 2005), with a series of nodal and other domain components. We first corroborated that addition of different fluorescent tags did not alter the fidelity of intracellular transport. We found that NF186 with a C-terminal EGFP tag (NF186-EGFP) was uniformly cotransported with NF186 with a C-terminal mKate2 tag (NF186-mKate2) in both anterogradely and retrogradely directed vesicles (Fig. S1, B–F). mKate2 is a bright, far-red fluorescent protein that, like EGFP, matures rapidly (Shcherbo et al., 2009). In contrast, NF186 tagged with other red fluorescent proteins (e.g., mCherry, mRFP, and DsRed) was not cotransported with NF186-EGFP (data not shown). Residual aggregation and/or delayed maturation of the latter three red fluorescent tags during biosynthesis presumably alters their recruitment into transport vesicles in the TGN (Snapp, 2005; Katayama et al., 2008; Kremers et al., 2011).

We next compared NF186-mKate2 with individual proteins tagged with EGFP to assess potential cotransport. Proteins analyzed included the nodal proteins NrCAM, KCNQ3, the sodium channel β subunits $Na_v\beta1$ and $Na_v\beta2$, the paranodal protein Caspr, and the internodal adhesion molecule CADM3/Necl1. Each of these EGFP-tagged components was appropriately targeted to its cognate domain upon myelination (Fig. 1 A), corroborating prior reports for several of these constructs (Dzhashiashvili et al., 2007; Zhang et al., 2012). We were unable to live image $Na_v1.2$, $Na_v1.6$, or AnkG as they were expressed during transport at levels below reliable detection in our system. Vesicle numbers were counted manually from kymographs of the live images (Fig. 1 C); transport direction was determined relative to the location of the neuronal soma. Images from red and green channels were acquired sequentially with a slight time delay. Because of this delay, the red and green channels were displaced for vesicles being actively transported (e.g., NrCAM vesicle b; Fig. 1 B), whereas they were aligned when vesicles were stationary (e.g., NrCAM vesicle a; Fig. 1 B).

In general, per previous reports (Nakata et al., 1998; Kaether et al., 2000), vesicles traveling anterogradely typically had an elongated tubulovesicular structure (mean ± SD: 1.54 ± 0.38 µm in length); those transported in the retrograde direction were rounder and much brighter (0.43 ± 0.11 µm in diameter). Transport velocities ranged from 0.34 ± 0.02 to 0.83 ± 0.04 µm/s (mean ± SEM) in the anterograde and from 0.39 ± 0.03 to 0.72 ± 0.06 µm/s in the retrograde direction (Table S1). These values are consistent with transport rates for a wide array of cargoes in the anterograde and retrograde directions driven by members of the kinesin-1 and dynein motor families, respectively (Maday et al., 2014). Of note, KIF5B/kinesin-1 has been reported to drive AnkG and thereby $Na_v$ channels in axons (Barry et al., 2014) and is therefore a candidate to transport the domain proteins studied here as well.

In the anterograde direction, all proteins were transported independently of NF186 with the exception of NrCAM, which was consistently cotransported with NF186 (see Fig. 1, B and D; and Videos 1 and 2). The percentages of each nodal component cotransported with NF186-mKate2/total number of mKate2-expressing vesicles are shown in Fig. 1 D. The corresponding values are NrCAM, 100%; $Na_v\beta2$, 5.6% ± 2.5%; $Na_v\beta1$, 0%; KCNQ3, 0%; Caspr, 0%; and Necl1, 0%. We also saw no cotransport in the anterograde direction in pairwise combinations of other domain components, exclusive of NF186 (Fig. S2, A–E). In further support of independent anterograde transport, transport velocities for several proteins ($Na_v\beta2$, KCNQ3, and Caspr) were significantly different (Table S1). Finally, we also live imaged pairwise combinations of several constructs using spinning disk confocal microscopy to record transport of mKate2 and EGFP constructs simultaneously rather than sequentially (Fig. S1, G–I). These results likewise corroborated the general patterns of anterograde transport described above.

These findings indicate that many anterogradely transported vesicles are likely to have distinct and limited membrane protein

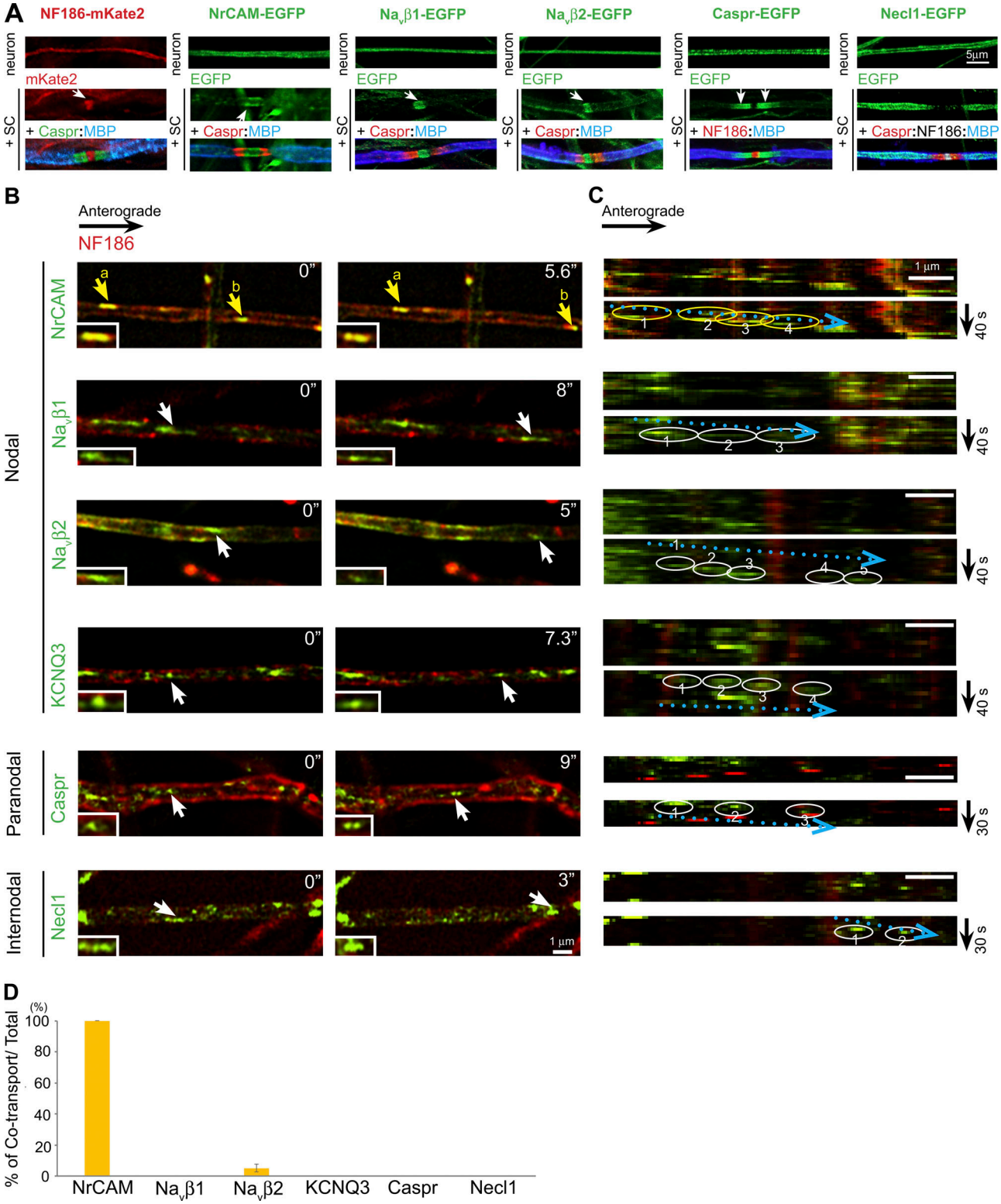


Figure 1. **Most domain components are independently transported in the anterograde direction**. **(A)** NF186-mKate2 and a series of EGFP-tagged constructs are expressed diffusely along axons in neuron-only cultures (upper row) and targeted to their appropriate domains (i.e., nodes, paranodes, internodes) in myelinating cocultures of neurons and Schwann cells (+SC, middle and lower rows). Nodes in the last two columns were identified by NF186 staining (red in the Caspr-EGFP cocultures and white in the Necl1-EGFP cocultures), and paranodes were identified by Caspr staining (except in the Caspr-EGFP cocultures); myelin segments were identified by MBP staining (MBP, blue). Bar: 5 µm. **(B)** Still images of domain components transported in the anterograde direction are shown. NF186-mKate2 (red) is compared with other components labeled with EGFP. Examples of vesicles containing EGFP-positive components are indicated by arrows; yellow indicates cotransport with mKate2 and white for EGFP alone. Two vesicles (a and b) that are colabeled for NF186 and NrCAM are indicated in the top panels. Inset shows higher power image of vesicle indicated by the arrows. Time of imaging (seconds) is indicated in each panel.

**(C)** Kymographs of anterogradely transported vesicles indicated by the arrows in the panels in A are shown. Trajectories of each vesicle are circled (yellow for cotransport, white for EGFP alone) and are numbered in temporal sequence. Dotted blue arrows indicate the direction of anterogradely transported vesicles. **(D)** Quantification of vesicles that colabeled for NF186 and the indicated EGFP-positive component versus the total number of anterogradely transported NF186 vesicles (average ± SEM) is shown. The numbers of axons counted are NrCAM, $n$ = 14; $Na_v\beta2$, $n$ = 14; $Na_v\beta1$, $n$ = 19; KCNQ3, $n$ = 10; Caspr, $n$ = 16; and Necl1, $n$ = 13. NF186 and NrCAM are uniformly cotransported, whereas other components exhibit negligible cotransport.

cargoes. They also indicate that node components are not preassembled for delivery to the axon. Rather, these components are likely carried via distinct vesicles derived from the trans-Golgi for independent transport to the axon for subsequent local assembly at the node.

### Domain components are cotransported in the retrograde direction following endocytosis

In contrast, there is significant cotransport of these various proteins in the retrograde direction (Fig. 2, A–C; and Videos 1 and 2), including nearly complete cotransport of NF186 and NrCAM. The percentages of vesicles with axonal proteins that are retrogradely cotransported with NF186-mKate2/total number of mKate2-expressing vesicles are NrCAM, 96.0% ± 2.2%; $Na_v\beta1$, 52.4% ± 6.2%; $Na_v\beta2$, 45.3% ± 10.7%; KCNQ3, 58.2% ± 8.6%; Caspr, 57% ± 10.0%; and Necl1, 52.4% ± 8.5% (Fig. 2 C). Similarly, pairwise comparisons of other domain components, exclusive of NF186, showed substantial cotransport (Fig. S2, C–E). We also corroborated that there is substantial retrograde cotransport for selected pairs of proteins using spinning disk confocal microscopy (Fig. S1, G and I).

We next examined the sources of the retrogradely transported proteins (i.e., whether they are internalized from the axonal membrane and/or represent vesicles undergoing bidirectional transport). For these studies, we analyzed an NF186 construct containing an AviTag epitope in its ectodomain and EGFP fused to its C terminus (Zhang et al., 2012). The AviTag epitope is biotinylated by BirA, a membrane-impermeable biotin ligase, only when the NF186 construct is expressed at the axon surface. Following biotinylation, neurons were live labeled with streptavidin-conjugated Alexa Fluor-568 and, after a 40-min delay, were dynamically imaged for up to 120 min. Alexa Fluor-568–labeled vesicles were only transported in the retrograde direction, indicating this pool of NF186-positive vesicles results from endocytosis. These results also suggest that the retrogradely cotransported cargoes likely result from coendocytosis.

While some proteins are routed to axons for anterograde transport following transcytosis (Lasiecka and Winckler, 2011), the absence of anterogradely transported vesicles labeled by avidin/Alexa Fluor-568 strongly suggests NF186 is not transcytosed. Further, anterogradely transported vesicles typically had a tubulovesicular structure (Fig. 1 B), suggesting they are directly derived from the TGN. Vesicles only labeled with EGFP were transported in both the anterograde and retrograde directions (Fig. 2 D); the latter likely represents vesicles that had internalized before biotinylation.

We next examined the fate of the internalized NF186. Cargoes trafficked into endosomes are sorted either back to the cell surface or to multivesicular bodies and then on to lysosomes for degradation (McMahon and Boucrot, 2011). Cargoes that progress through the latter endocytic pathway are subject to an increasingly acidic environment of the late endosomes and lysosomes (Casey et al., 2010), which can be monitored with pH-sensitive probes. We used pHrodo Red conjugated to streptavidin to analyze the internalized AviTag-NF186–containing vesicles. We observed that many of the NF186-containing, retrogradely transported vesicles were pHrodo-positive; an example is shown in the still image and the corresponding kymograph in Fig. 2 E. Similarly, many of the retrogradely transported NF186-positive vesicles were colabeled by Lysotracker (i.e., mean ± SEM: 45.5% ± 5.17%); an example is shown in Fig. S2 F.

Together, these results indicate that a substantial proportion of the retrogradely transported NF186 and the cotransported cargoes (Fig. 2 C) are endocytosed and destined for lysosomal degradation. They do not exclude that a portion of the endocytosed NF186 does not enter these acidic endomembranous compartments but rather is recycled back to the plasma membrane, as is known to occur in dendrites (Yap et al., 2012).

### Effects of myelination on vesicular transport

We previously showed that NF186 is diffusion trapped from a preexisting surface pool during node assembly, whereas it is replenished by transport from an intracellular pool during node maintenance (Zhang et al., 2012). These findings raise the possibility that myelination may alter how NF186 or other components of the node are sorted and transported to this site. To address this, we investigated whether the patterns of vesicular transport or the total number of vesicles was affected by the onset of myelination. We first infected neuron-only cultures with viral constructs, added Schwann cells, and after several days under myelinating conditions, live imaged the cocultures.

In general, the overall patterns of transport in the cocultures were quite similar to those of neuron-only cultures (i.e., nodal components were largely transported independently in the anterograde direction and substantially cotransported in the retrograde direction). Pairwise comparisons of transport between NF186-mKate2 and either EGFP-tagged $Na_v\beta1$, $Na_v\beta2$, or KCNQ3 are shown in Fig. 3. In the anterograde direction, the percentages of vesicles exhibiting cotransport with NF186-mKate2 were $Na_v\beta1$, 13.9% ± 4.7% (mean ± SEM); $Na_v\beta2$, 7.6% ± 3.0%; and KCNQ3, 0.6% ± 0.6% (Fig. 3, A and B). In the retrograde direction, the percentages of cotransport with NF186-mKate2 were $Na_v\beta1$, 68.9% ± 4.9%; $Na_v\beta2$, 68.7% ± 4.0%; and KCNQ3, 45.9% ± 5.8% (Fig. 3, D and E). Thus, the overall patterns of transport were not affected at the onset of myelination in these cultures. Whether these trafficking patterns persist in much older cocultures after myelination is largely complete will be of interest for future study.

The additional time required for myelination meant that neurons in these cocultures were older, i.e., 17–21 days in vitro

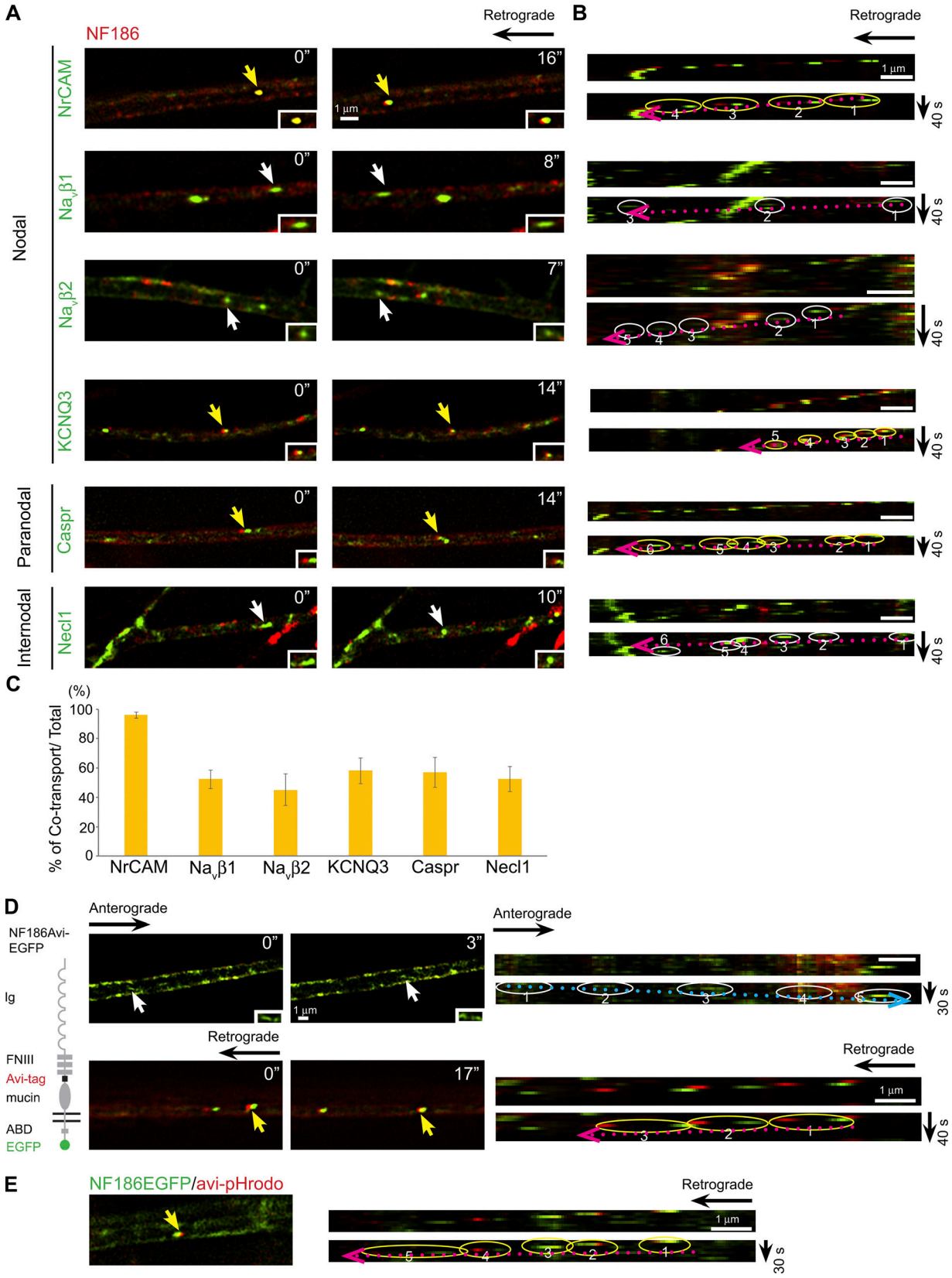


Figure 2. **Domain components are substantially cotransported in the retrograde direction following endocytosis. (A)** Still images of domain components transported in the retrograde direction are shown. NF186 tagged with mKate2 (red) is compared with other components labeled with EGFP. Yellow arrows indicate vesicles with EGFP-tagged components that are cotransported with NF186-mKate2; white arrows indicate vesicles labeled with EGFP alone. Insets show higher power images of vesicles indicated by the arrows. Time of imaging (seconds) is indicated in each panel. **(B)** Kymographs of the retrogradely

transported vesicles indicated by the arrows in the panels in A are shown. Trajectories of each vesicle are circled (yellow for cotransport, white for EGFP alone with the retrograde direction indicated by the dotted red arrows); vesicle positions are numbered in temporal sequence. **(C)** Quantification of vesicles that colabel for NF186 and the indicated EGFP+ component versus the total number of retrogradely transported NF186 vesicles (average ± SEM) is shown. The numbers of axons counted were NrCAM, $n$ = 15; $Na_V\beta2$, $n$ = 18; $Na_V\beta1$, $n$ = 20; KCNQ3, $n$ = 17; Caspr, $n$ = 15; and Necl1, $n$ = 16. NF186 is uniformly cotransported with NrCAM and substantially cotranported with all other components as shown. **(D)** Representative micrographs show biotinylated Avi-tagged NF186-EGFP labeled with streptavidin 568 and then live imaged. Upper rows show anterograde vesicles (white arrow, white circles); lower rows show retrograde vesicles (yellow arrow, yellow circle). Insets show higher power images of vesicles indicated by the arrows. Time of imaging (seconds) is indicated in each panel. Dotted arrows indicate the direction of transport (i.e., blue, anterograde and red, retrograde). The separation of red and green markers in the retrograde vesicles reflects ongoing transport during the change in the emission filters. **(E)** Avi-tagged NF186 EGFP transported in the retrograde direction colabeled with pHrodo Red Avidin, indicating it is an acidic compartment. In the kymograph, the vesicle trajectory is circled (yellow for cotransport) and numbered in temporal sequence; the dotted red arrow indicates the retrograde direction. Scale bars: 1 µm.

(DIV) and generally exhibited fewer numbers of vesicles labeled with virally encoded constructs. Of interest, the numbers of transport vesicles were significantly greater in neurons cocultured with Schwann cells under myelinating conditions than in age-matched neuron-only cultures. This was true whether the tagged constructs were constitutively or inducibly expressed under control of the FUGW or the pSLIK lentiviral vectors, respectively (Fig. 3 C and F–H). Vitamin C/ascorbate was added to cocultures to promote myelination by enhancing basal lamina formation (Eldridge et al., 1987); it is also known to promote demethylation of DNA and histones (Young et al., 2015; Camarena and Wang, 2016). We therefore added it to neuron-only cultures as a further control, with no evident increase in the numbers of labeled vesicles. These results indicate that the transition to myelination, even after just a few days, increased the numbers of labeled vesicles. It is not yet known if this increase results from a general elevation in neuronal transcription, increased translation of these constructs, and/or increased assembly of vesicles generated from the TGN.

### Co-sorting of NF186 and NrCAM into transport vesicles is mediated by their cytoplasmic domains

A striking finding is the consistent cotransport of NF186 and NrCAM in both the anterograde and retrograde directions. Both CAMs are members of the Ig superfamily (i.e., IgCAMs) and have similar domain organizations (Volkmer at al., 1992; Fig. 4 A). To address the role of the cytoplasmic domain in the cosorting of these proteins, we first compared the extent of vesicular cotransport of NF186 with that of Intercellular Adhesion Molecule (ICAM; Fig. 4, B–E), a lymphocyte IgCAM that is diffusely distributed on myelinated axons after heterologous expression in neurons (Dzhashiashvili et al., 2007). As expected, there was almost no cotransport of NF186-mKate2 with ICAM-EGFP in the anterograde direction (1.7% ± 1.7%) and only modest cotransport in the retrograde direction (29.8% ± 7.5%).

We next compared sorting of NF186-mKate2 to ICAM/NF186-EGFP, a chimeric construct containing the ectodomain and transmembrane segments of ICAM fused to the cytoplasmic domain of NF186 (Fig. 4 A). We previously showed this construct is targeted to mature nodes in a transport-dependent fashion (Zhang et al., 2012). ICAM/NF186 is significantly cotransported with NF186 in the anterograde direction (87.3% ± 5.1%; Fig. 4 C), indicating the key role of the cytoplasmic domain of NF186 in its sorting to its cognate transport vesicles. ICAM/NF186 was also substantially cotransported with NF186 in the retrograde direction (82.6% ± 4.7%; Fig. 4 E). This latter result suggests the cytoplasmic domain of NF186 contributes to selective cointernalization at the plasma membrane.

### AnkG regulates NF186 cotransport and trafficking

The cytoplasmic segments of both NrCAM and NF186 harbor a conserved five–amino acid sequence, FIGQY, which is part of the ankyrin binding domain (ABD; Zhang et al., 1998). To assess if the ABD is required for cotransport of NF186 and NrCAM, we did pairwise comparisons of the transport of an NF186 construct containing a deletion of the ABD (NFΔABD) with wt NF186 or wt NrCAM (Fig. 4, F–I). Deletion of the ABD substantially reduced the extent of anterograde cotransport. Thus, anterograde cotransport of NF186ΔABD-EGFP with NF186-mKate2 was 31.9% ± 6.2% and with NrCAM-mKate2 was 39.1% ± 8.3% (Fig. 4 G). Potentially, other sequences in the cytoplasmic domain of NF186, such as the aromatic and negatively charged residues ($Ser^{56}$–$Tyr^{81}$) may contribute to AnkG interactions (Zhang et al., 1998) and account for this residual anterograde cosorting.

In the retrograde direction, there were more modest reductions of cotransport (i.e., with NF186, 66.8% ± 4.9%, and with NrCAM, 74.4% ± 7.2%; Fig. 4 I). These effects on retrograde cotransport may reflect changes in the internalization of NF186ΔABD–EGFP at the plasma membrane. Interactions of the FIGQY segment are regulated by phosphorylation: nonphospho-FIGQY binds to AnkG, whereas phospho-FIGQY binds to doublecortin (Kizhatil et al., 2002), which functions as an endocytic adaptor that promotes NF186 internalization (Yap et al., 2012; Yap et al., 2018). Therefore, loss of this ABD sequence would be expected to disrupt both AnkG and doublecortin interactions, impairing its stability at the membrane but also its internalization, respectively.

To further address a role of AnkG, we examined NF186 transport in neurons after shRNA knockdown of AnkG. We employed two different lentiviral shRNA constructs (sh1AnkG and sh2AnkG), each of which is known to essentially eliminate all AnkG isoforms without affecting AnkB levels (Dzhashiashvili et al., 2007); as a further control, we used a scrambled shRNA (scr) construct. Neurons harboring these shRNA constructs were identified by their expression of GFP, which is also driven by the lentiviral vector. Knockdown of AnkG did not significantly affect Necl1 transport (Fig. 5, A and B) as expected, given the lack of interactions between these two proteins. In contrast, the numbers of NF186-mKate2–positive anterogradely transported vesicles were substantially reduced with AnkG knockdown but not

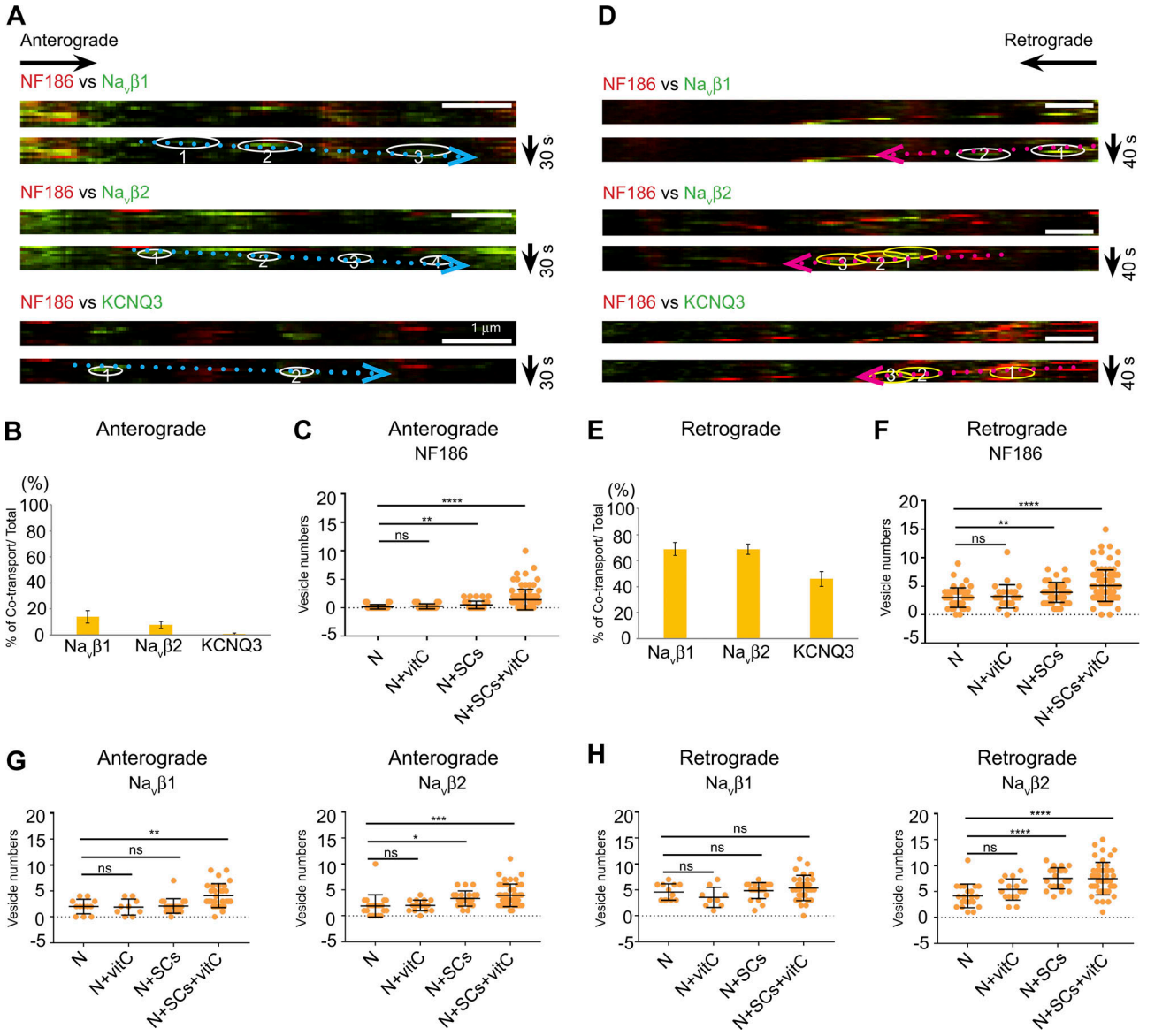


Figure 3. **Schwann cells' interactions with axons do not alter the patterns of bidirectional transport but increase the numbers of labeled transport vesicles. (A and D)** Representative images from kymographs of vesicles transported in the anterograde (A) and retrograde (D) directions in Schwann cell/neuron cocultures are highlighted by dotted blue and red arrows, respectively. White circles highlight vesicles with just EGFP-tagged components; yellow circles show vesicles that cotransport EGFP components and NF186-mKate2. Bars: 1 µm. **(B)** Quantification of EGFP+ vesicles that colabel with NF186 versus the total number of anterogradely transported NF186-positive vesicles. The numbers of axons analyzed were Na$_v$β1, *n* = 30; Na$_v$β2, *n* = 44; and KCNQ3, *n* = 22. Error bars indicate mean ± SEM. **(C)** Quantification of anterogradely transported NF186-positive vesicles in age-matched neurons (N) cultured with or without Schwann cells (SCs) and ascorbate (vitC). The mean ± SD for each condition is N only 0.24 ± 0.43 (*n* = 36); N with vitC, 0.22 ± 0.51 (*n* = 36); N with SCs, 0.40 ± 0.60 (*n* = 54); and N with SCs and vitC, 1.43 ± 1.78 (*n* = 97). **(E)** Quantification of EGFP+ vesicles that colabel with NF186 versus the total number of retrogradely transported NF186-positive vesicles. The numbers of axons analyzed were Na$_v$β1, *n* = 30; Na$_v$β2, *n* = 44; and KCNQ3, *n* = 22. Error bars indicate mean ± SEM. **(F)** Quantification of retrogradely transported NF186-positive vesicles in age-matched neurons (N) cultured with or without Schwann cells and ascorbate. The mean ± SD for each condition is N only, 3.00 ± 1.72 (*n* = 46); N with vitC, 3.22 ± 2.04 (*n* = 27); N with SC, 3.92 ± 1.75 (*n* = 53); and N with SCs and vitC, 5.11 ± 2.77 (*n* = 96). **(G)** Quantification of anterogradely transported Na$_v$β1 and Na$_v$β2 vesicle numbers in age-matched neurons (N) cultured with or without Schwann cells and ascorbate (C). Na$_v$β1 vesicle numbers were N only, 2.00 ± 1.41 (*n* = 12); N with vitC, 1.89 ± 1.54 (*n* = 9); N with SC, 2.10 ± 1.41 (*n* = 20); and N with SCs and vitC, 4.10 ± 2.29 (*n* = 31). Na$_v$β2 vesicle numbers were N only, 1.90 ± 2.14 (*n* = 21); N with vitC, 2.00 ± 1.03 (*n* = 16); N with SCs, 3.33 ± 1.46 (*n* = 22); and N with SCs and vitC, 3.95 ± 2.17 (*n* = 44). **(H)** Quantification of retrogradely transported Na$_v$β1 and Na$_v$β2 vesicle numbers in age-matched neurons (N) cultured with or without Schwann cells and ascorbate (C). Na$_v$β1 vesicle numbers were N only, 4.58 ± 1.56 (*n* = 12); N with vitC, 3.56 ± 1.94 (*n* = 9); N with SCs, 4.85 ± 1.53 (*n* = 20); and N with SCs and vitC, 5.40 ± 2.42 (*n* = 30). Na$_v$β1 vesicle numbers were N only, 4.14 ± 2.29 (*n* = 21); N with vitC, 5.38 ± 2.06 (*n* = 16); N with SCs, 7.52 ± 2.04 (*n* = 21); and N with SCs and vitC, 7.48 ± 3.13 (*n* = 44). In panels C and F–H, statistical significance was determined by two-tailed Student's *t* test for unpaired data, with asterisks indicating P values of ****, P < 0.001; ***, P < 0.005; **, P < 0.01; and *, P < 0.05; ns, not significant.

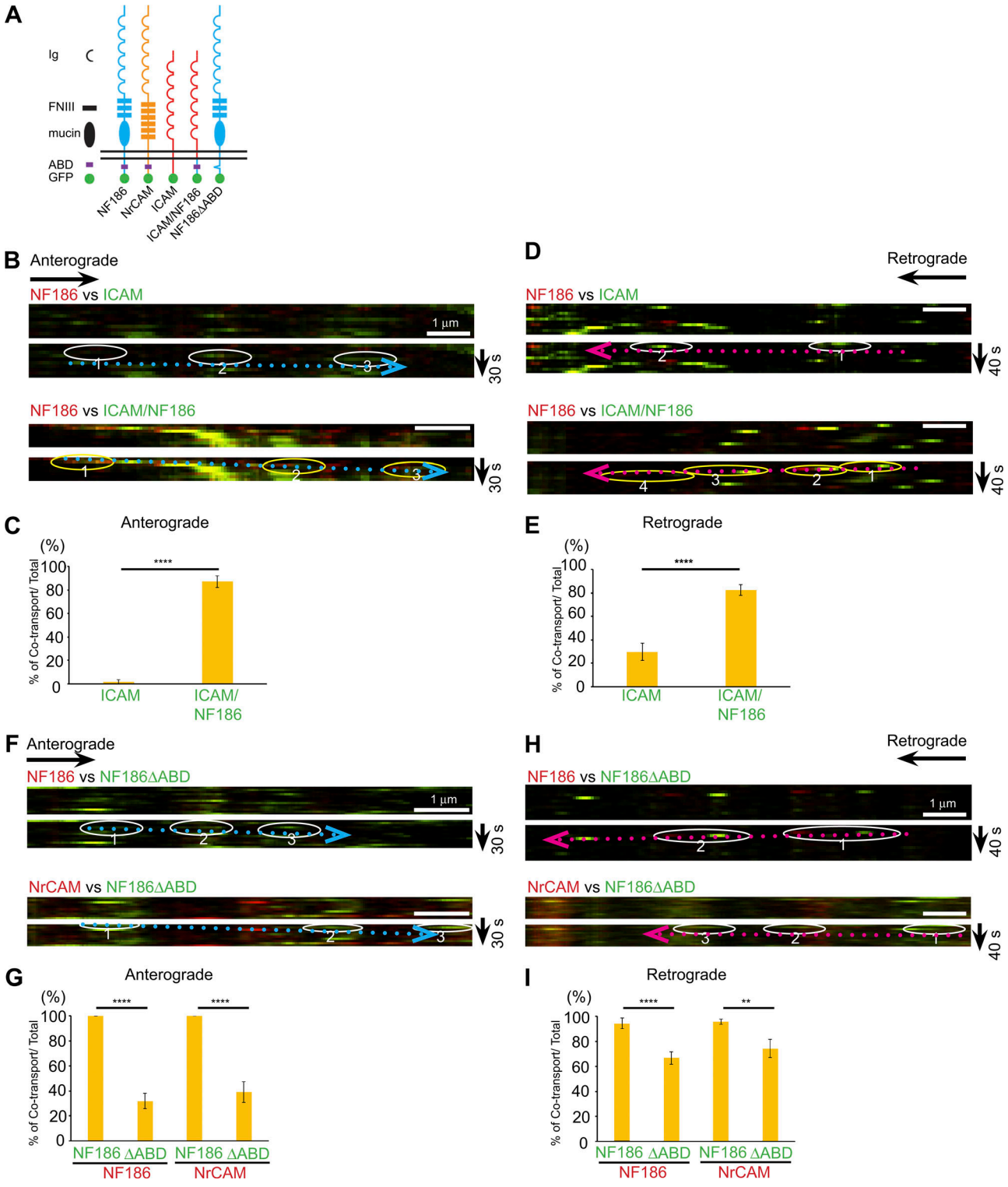


Figure 4. **Cotransport of NF186 and NrCAM depends on their ABD. (A)** Schematic diagram of chimeric constructs and their domain organizations. **(B and D)** Kymographs of neurons expressing NF186-mKate2 (red) and either ICAM (green; top panels) or NF/ICAM (green; bottom panels) in the anterograde (B) or retrograde (D) direction. **(C and E)** Quantification of vesicles that cotransport NF186-mKate2 with ICAM or NF/ICAM versus total numbers of NF186-positive vesicles in the anterograde (C) and retrograde (E) directions. Numbers of axons analyzed in the anterograde direction were ICAM-EGFP, *n* = 15 and ICAM/NF186, *n* = 17; in the retrograde direction, ICAM-EGFP, *n* = 20, and ICAM/NF186, *n* = 30. Statistical significance was determined by two-tailed Welch's *t* test for unpaired data, with asterisks indicating a P value of ****, P < 0.001. Error bars indicate mean ± SEM. **(F and H)** Upper duplicate kymographs show trafficking of vesicles in neurons infected with NF186-mKate2 (red) and NF186ΔABD-EGFP (green) in the anterograde (F) and retrograde (H) directions; in each case, an example of a transport vesicle is circled below. The bottom duplicate kymographs show trafficking of vesicles in neurons infected with NrCAM-mKate2 (red) and NF186ΔABD-EGFP (green) with an example shown circled below. Scale bars, 1 µm. **(G and I)** Bar graphs show the percentages of cotransported vesicles

versus total NF186-mKate2 or NrCAM-mKate2 vesicles in the anterograde (G) and retrograde (I) directions. Numbers of axons analyzed in the anterograde direction: NF186ΔABD-EGFP with NF186-mKate2, $n$ = 19, and with NrCAM-mKate2, $n$ = 13; in the retrograde direction: NF186ΔABD-EGFP with NF186-mKate2, $n$ = 20, and with NrCAM-mKate2, $n$ = 14. Statistical significance was determined by two-tailed Welch's $t$ test for unpaired data, with asterisks indicating P values of ****, P < 0.001 and **, P < 0.01. Error bars indicate mean ± SEM.

by the scr construct (i.e., sh1AnkG, 26.7% ± 4.9%; sh2AnkG, 28.0% ± 4.2% vs. scr, 100.0% ± 10.4%; Fig. 5 A). There was also a modest decrease in the numbers of retrogradely transported NF186-positive vesicles (sh1AnkG, 73.3% ± 10.4%; sh2AnkG, 71.1% ± 5.8% vs. scr, 100.2% ± 8.4%; Fig. 5 B).

Thus, results with the NF186ΔABD construct and AnkG knockdown together implicate AnkG in NF186 trafficking, potentially by regulating its sorting and/or egress from the TGN and its internalization at the plasma membrane. Consistent with a role at the TGN, binding of the newly synthesized E-cadherin–β-catenin complex in epithelial cells to AnkG in the TGN is required for its exit from this compartment (Kizhatil et al., 2007). These results suggest that binding of NF186 and NrCAM to AnkG in the TGN of neurons may likewise direct their sorting and egress. The specific AnkG isoform(s) that mediates these effects in neurons is not known. AnkG has several splice variants, including $AnkG_{480}$ and $AnkG_{270}$, which are neuron specific and predominantly expressed at the axon initial segment and nodes of Ranvier (Zhang and Bennett, 1998), and $AnkG_{190}$, which is also expressed in neurons (Smith et al., 2014). Future studies using isoform-specific knockouts/knockdowns will be useful to elucidate further the isoform(s) and mechanisms involved.

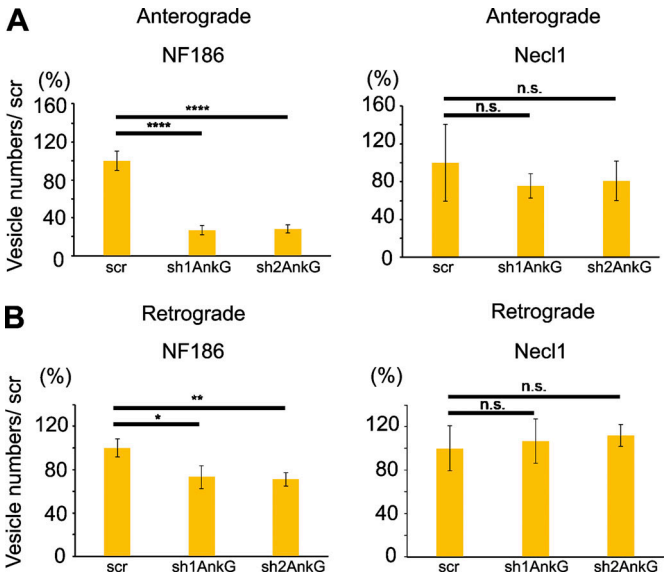


Figure 5. **AnkG regulates the numbers of NF186-positive transport vesicles. (A and B)** Quantification of vesicle numbers in control versus AnkG knockdown cultures in the anterograde (A) and retrograde (B) directions is shown. The total number of axons analyzed were NF186 with sh1AnkG, $n$ = 22, sh2AnkG, $n$ = 28, and scr, $n$ = 27; and Necl1 with sh1AnkG, $n$ = 6, sh2AnkG, $n$ = 5, and scr, $n$ = 5. Statistical significance was determined by two-tailed Student's $t$ test for unpaired data, with asterisks indicating P values of ****, P < 0.001; **, P < 0.01; and *, P < 0.05; n.s., not significant.

Our data also suggest that AnkG may regulate NF186 and NrCAM vesicle transport. This is consistent with its reported role in the transport of $Na_v1.2$ (Barry et al., 2014) and cyclic nucleotide-gated (Kizhatil et al., 2009) channels and the selective delivery of $Na_v1.6$ to the axon initial segment (Akin et al., 2015). In potential support, the transport velocity of NF186 that lacks the ABD is increased (Table S1), with no change in overall vesicle movement in the anterograde and retrograde directions (data not shown). NF186 may bind indirectly via AnkG to motor proteins such as KIF5B (Barry et al., 2014) and may bind to other motor proteins in the absence of this interaction. Future investigations will be necessary to clarify further the potential roles of AnkG in TGN sorting versus axonal transport.

In summary, we report that anterogradely transported vesicles preferentially carry single axonal domain proteins, indicating significant diversity of such vesicles. The notion of separate transport vesicles with specific cargoes for distinct destinations in neurons is consistent with evidence, for example, that Kv channels targeted to different dendritic subdomains are sorted into separate vesicles in the Golgi (Jensen et al., 2014). There are exceptions to these findings of independent transport. Caspr obligately forms a cis-complex with contactin in the ER, with subsequent cotransport throughout the endomembrane system (Faivre-Sarrailh et al., 2000; Gollan et al., 2003). AnkG has been reported to be cotransported with $Na_v1.2$ into axons (Barry et al., 2014), and our data also indicate that NrCAM and NF186 are cotransported.

Classically, sorting of transmembrane cargoes into transport vesicles is thought to occur in the TGN via sorting signals in the cytosolic tails of the cargoes that are recognized by various adaptor proteins (Bentley and Banker, 2016; Guo et al., 2014), including members of the AP family (e.g., AP1) in coordination with Arf proteins, phospholipids, and coat proteins (Guardia et al., 2018; Tan and Gleeson, 2019). A recent report indicates neuronal transmembrane proteins may also segregate within the Golgi itself, before the TGN, for transport to the plasma membrane; this segregation occurs via their luminal or transmembrane sequences and is independent of cytosolic sorting signals and their cognate adaptors (Chen et al., 2017). This alternative pathway is an attractive candidate to account for the diversity of transport vesicles observed here. Future studies that delineate the mechanisms of sorting and transport of these various axonal proteins will be of considerable interest to elucidate further how the distinctive subdomains of axons are established.

## Materials and methods

### Animals

Timed pregnant Sprague Dawley rats were provided by commercial vendors (Charles River or Taconic). All animal

experiments were performed in compliance with the relevant policies and institutional guidelines issued by the New York University School of Medicine Institutional Animal Care and Use Committee.

### cDNA and lentiviral constructs

The pSLIK doxycycline-inducible vector system (Shin et al., 2006), modified as described (Zhang et al., 2012), was used as the vector for almost all cDNA constructs. Constitutive expression of NF186-mKate2 was driven by FUGW (Lois et al., 2002). Various fluorescently tagged constructs (i.e., NF186, NF186ΔABD, NF186avi, NrCAM, KCNQ3, ICAM, ICAM/NF186, and an shRNA construct to AnkG and a corresponding scr sequence) have all been described previously (Dzhashiashvili et al., 2007; Zhang et al., 2012). Sodium channel β1 and β2 subunit cDNA was provided by Dr. L. Isom (University of Michigan, Ann Arbor, MI), human Caspr cDNA was provided by Dr. E. Peles (Weizmann Institute, Rehovot, Israel), and a KCNQ3 cDNA construct was provided by Dr. M. Shapiro (University of Texas Health, San Antonio, TX); rat Necl1/Cadm3 cDNA was generated as described (Maurel et al., 2007).

### Cell culture

Rat DRG neurons cultured alone or with rat Schwann cells were established as described previously (Einheber et al., 1993), with modest modifications. Rat DRGs were removed from either E16 rat dissociated with 0.25% trypsin, plated onto a poly-L-lysine/laminin–coated glass-bottom dish (MatTek Corporation) and maintained in neurobasal (NB) media (2% B-27, 2 mM L-glutamine, 0.4% glucose, and 50 ng/ml 2.5S nerve growth factor in neurobasal medium). Non-neuronal cells were eliminated with antimitotic treatment with floxuridine. In some cases, Schwann cells were added to the DRG neuron cultures and maintained in C media (10% fetal bovine serum, 50 ng/ml 2.5S nerve growth factor, 0.4% glucose, and 20 mM L-glutamine in minimum essential medium) for 5 d. 50 µg/ml ascorbic acid was then added to initiate myelination.

### Viral production and lentiviral infection

293FT cells (Invitrogen) were transfected with the doxycycline-inducible vector pSLIK and FUGW lentiviral constructs and helper plasmids Δ8.9 and VSVg using the LipoD293 in vitro DNA transfection reagent (SignaGen Laboratories). Viral supernatants were collected 48 h after transfection, aliquoted, and stored at −80°C until used. For analysis of transport in neuron-only cultures, DRG neurons were infected with viral stocks 1 d after plating into culture. For dual lentiviral infections, one viral supernatant was added to neuron cultures and incubated for 24 h; cultures were then infected with the second construct and incubated for an additional 24 h. This provided higher efficiencies of dual infections than did simultaneous infection with both constructs. In studies examining cotransport at the onset of myelination, neuron cultures were infected 1 d after plating with pSLIK constructs and the following day with FUGW vector driving NF186-mKate2. All constructs subcloned in the pSLIK vector were induced with 2 µg/ml doxycycline for 1–2 d before live imaging.

### Surface biotinylation of neurons and imaging of acidic compartments

DRG neurons expressing AviTag-NF186 at DIV 5–8 were rinsed with biotinylation media (1% FBS C medium, 5 mM $Mg^{2+}$, and 10 mM Hepes) then incubated with the biotinylation solution containing 0.3 µM BirA ligase, 10 µM d-biotin, and 1 mM ATP (Avidity) in biotinylation medium for 10 min at 37°C. Cultures were rinsed with 1% FBS C medium with 10 mM Hepes and incubated with 5 µg/ml streptavidin–Alexa Fluor-568 (Invitrogen) or 4 µg/ml pHrodo Red Avidin (Invitrogen) for 5 min at RT. After washing, cultures were live imaged. In other studies, DRG neurons were incubated with 50 nM LysoTracker Red DND-99 (ThermoFisher Scientific) in NB medium for 1 h at 37°C.

### Antibodies and immunohistochemistry

Cultures were stained with a chicken antibody against myelin basic protein (MBP; 1:100; MilliporeSigma), a guinea pig antibody against Caspr (1:3,000; M. Bhat, University of Texas Health, San Antonio, TX), a mouse monoclonal antibody against neurofascin (A12/A18, specific for nodal NF, 1:3,000; NeuroMab), a rabbit antibody against tRFP (1:15,000; Evrogen), and a goat antibody against GFP (1:4,000; Bio-Rad). Secondary donkey antibodies conjugated to Rhodamine Red-X, DyLight 405, and Alexa Fluor-488, -568, and -680 were obtained from Jackson ImmunoResearch Laboratories and used at 1:1,000 dilution each.

Cocultures were fixed in 4% PFA for 10 min. Samples were permeabilized in 100% methanol for 10 min at −20°C, incubated with blocking solution containing 1% donkey serum, 5% bovine serum albumin, and 0.2% Triton-X in PBS for 1 h, and incubated with primary antibodies overnight at 4°C. Samples were washed with PBS, incubated with secondary antibodies for 2 h at RT, washed with PBS, and mounted in Fluoromount G (SouthernBiotech) for imaging.

### Live imaging of vesicle transport and confocal microscopy

Live imaging was done principally with a Nikon Eclipse Ti-E microscope with a Nikon plan Apo Lambda 100×/1.45 NA objective unless otherwise mentioned. NIS-Elements Advanced Research Software (Nikon) was used for image processing after data acquisition. During live imaging, cultures were maintained in phenol red-free NB or C media buffered with 10 mM Hepes at 37°C. Images were captured at 2-s intervals for 2 min with CCD cameras (Clara; Andor Technology and DS-Qi2; Nikon). Channels were captured sequentially with a slight time delay secondary to filter wheel switching. In some cases, we also used Nikon W1 spinning disk confocal microscopy with an SR HP Plan Apo 100×/1.35 NA objective for live imaging. In the latter case, images were collected at 0.2 s over 2 min with both channels captured simultaneously with two EMCCD cameras (Andor 888; Andor Technology). Images of fixed cocultures were captured with a Zeiss LMS800 confocal microscope with Zeiss Plan-Neofluar 10×/0.3 NA and APOCHROMAT 63×/1.4 NA objectives.

### Quantification of vesicles and statistical analysis

The direction of vesicle transport for each axon was determined by the direction relative to that of the neuronal soma. Vesicle

numbers in each direction were counted using kymograph software (NIS-Elements Advanced Research Software). To compare vesicle numbers, kymographs were generated by live imaging 15-µm sections of axons for 2 min. As some anterograde vesicles were of limited brightness, all quantitative results were confirmed by using ImageJ Manual Tracking. Cotransport was measured by pairwise comparisons of EGFP versus mKate2 labeling of the vesicles within individual axons (with only one axon typically measured per neuron). Total vesicles counted in comparisons with NF186-mKate2 are provided in Table S1. We then averaged results from separate axons to determine the extent of cotransport for each construct. Imaging was performed during at least three and up to eight separate sessions, each on separate days and typically on separate cultures. Cotransport rates that we calculated by averaging results from imaging sessions were comparable to those measured by averages of axons. Statistical significance was assessed with either the two-tailed Welch's *t* test or the two-tailed Student's *t* test for unpaired data using Excel and GraphPad Prism software. Data distribution was assumed to be normal, but this was not formally tested.

The average velocities of vesicles in each direction were measured by using ImageJ Manual Tracking. Kymographs from spinning disk were generated by using ImageJ macros (NYU Langone Microscopy Core). Sizes of anterograde and retrograde vesicles were averaged from measurements of 26 separate vesicles using NIS-Elements Advanced Research Software.

### Online supplemental material

Fig. S1 demonstrates that NF186-mKate2 and NF186-EGFP are uniformly cotransported bidirectionally and shows spinning disk confocal images. Fig. S2 shows examples of transport for other combinations of axonal components. Table S1 shows the velocities of anterogradely and retrogradely transported EGFP-labeled proteins. Video 1 shows bidirectional transport of NF186-mKate2 and $Na_v\beta2$-EGFP. Video 2 shows retrograde transport of NF186-mKate2 and Caspr-EGFP.

## Acknowledgments

We thank Erik Snapp for kindly providing the mKate2 construct and advice on the use of fluorophores for live imaging and Michael Cammer at the New York University Langone Microscopy Core for experimental and technical support with imaging analysis.

This research was supported by a National Institutes of Health grant (NS043474) to J.L. Salzer. Y. Bekku was a recipient of a postdoctoral fellowship from the National Multiple Sclerosis Society.

The authors declare no competing financial interests.

Author contributions: Y. Bekku and J.L. Salzer designed the experiments. Y. Bekku carried out and analyzed all experiments. Y. Bekku and J.L. Salzer co-wrote and edited the manuscript.

Submitted: 12 June 2019
Revised: 28 January 2020
Accepted: 25 March 2020

## References

Akin, E.J., L. Solé, S.D. Dib-Hajj, S.G. Waxman, and M.M. Tamkun. 2015. Preferential targeting of Nav1.6 voltage-gated Na+ Channels to the axon initial segment during development. *PLoS One.* 10:e0124397. https://doi.org/10.1371/journal.pone.0124397

Barry, J., Y. Gu, P. Jukkola, B. O'Neill, H. Gu, P.J. Mohler, K.T. Rajamani, and C. Gu. 2014. Ankyrin-G directly binds to kinesin-1 to transport voltage-gated Na+ channels into axons. *Dev. Cell.* 28:117–131. https://doi.org/10.1016/j.devcel.2013.11.023

Bentley, M., and G. Banker. 2016. The cellular mechanisms that maintain neuronal polarity. *Nat. Rev. Neurosci.* 17:611–622. https://doi.org/10.1038/nrn.2016.100

Camarena, V., and G. Wang. 2016. The epigenetic role of vitamin C in health and disease. *Cell. Mol. Life Sci.* 73:1645–1658. https://doi.org/10.1007/s00018-016-2145-x

Casey, J.R., S. Grinstein, and J. Orlowski. 2010. Sensors and regulators of intracellular pH. *Nat. Rev. Mol. Cell Biol.* 11:50–61. https://doi.org/10.1038/nrm2820

Chen, Y., D.C. Gershlick, S.Y. Park, and J.S. Bonifacino. 2017. Segregation in the Golgi complex precedes export of endolysosomal proteins in distinct transport carriers. *J. Cell Biol.* 216:4141–4151. https://doi.org/10.1083/jcb.201707172

Dzhashiashvili, Y., Y. Zhang, J. Galinska, I. Lam, M. Grumet, and J.L. Salzer. 2007. Nodes of Ranvier and axon initial segments are ankyrin G-dependent domains that assemble by distinct mechanisms. *J. Cell Biol.* 177:857–870. https://doi.org/10.1083/jcb.200612012

Einheber, S., T.A. Milner, F. Giancotti, and J.L. Salzer. 1993. Axonal regulation of Schwann cell integrin expression suggests a role for alpha 6 beta 4 in myelination. *J. Cell Biol.* 123:1223–1236. https://doi.org/10.1083/jcb.123.5.1223

Eldridge, C.F., M.B. Bunge, R.P. Bunge, and P.M. Wood. 1987. Differentiation of axon-related Schwann cells in vitro. I. Ascorbic acid regulates basal lamina assembly and myelin formation. *J. Cell Biol.* 105:1023–1034. https://doi.org/10.1083/jcb.105.2.1023

Faivre-Sarrailh, C., F. Gauthier, N. Denisenko-Nehrbass, A. Le Bivic, G. Rougon, and J.A. Girault. 2000. The glycosylphosphatidyl inositol-anchored adhesion molecule F3/contactin is required for surface transport of paranodin/contactin-associated protein (caspr). *J. Cell Biol.* 149:491–502. https://doi.org/10.1083/jcb.149.2.491

Gollan, L., D. Salomon, J.L. Salzer, and E. Peles. 2003. Caspr regulates the processing of contactin and inhibits its binding to neurofascin. *J. Cell Biol.* 163:1213–1218. https://doi.org/10.1083/jcb.200309147

Guardia, C.M., R. De Pace, R. Mattera, and J.S. Bonifacino. 2018. Neuronal functions of adaptor complexes involved in protein sorting. *Curr. Opin. Neurobiol.* 51:103–110. https://doi.org/10.1016/j.conb.2018.02.021

Guo, Y., D.W. Sirkis, and R. Schekman. 2014. Protein sorting at the trans-Golgi network. *Annu. Rev. Cell Dev. Biol.* 30:169–206. https://doi.org/10.1146/annurev-cellbio-100913-013012

Jensen, C.S., S. Watanabe, H.B. Rasmussen, N. Schmitt, S.P. Olesen, N.A. Frost, T.A. Blanpied, and H. Misonou. 2014. Specific sorting and post-Golgi trafficking of dendritic potassium channels in living neurons. *J. Biol. Chem.* 289:10566–10581. https://doi.org/10.1074/jbc.M113.534495

Kaether, C., P. Skehel, and C.G. Dotti. 2000. Axonal membrane proteins are transported in distinct carriers: a two-color video microscopy study in cultured hippocampal neurons. *Mol. Biol. Cell.* 11:1213–1224. https://doi.org/10.1091/mbc.11.4.1213

Katayama, H., A. Yamamoto, N. Mizushima, T. Yoshimori, and A. Miyawaki. 2008. GFP-like proteins stably accumulate in lysosomes. *Cell Struct. Funct.* 33:1–12. https://doi.org/10.1247/csf.07011

Kizhatil, K., Y.X. Wu, A. Sen, and V. Bennett. 2002. A new activity of doublecortin in recognition of the phospho-FIGQY tyrosine in the cytoplasmic domain of neurofascin. *J. Neurosci.* 22:7948–7958. https://doi.org/10.1523/JNEUROSCI.22-18-07948.2002

Kizhatil, K., J.Q. Davis, L. Davis, J. Hoffman, B.L. Hogan, and V. Bennett. 2007. Ankyrin-G is a molecular partner of E-cadherin in epithelial cells and early embryos. *J. Biol. Chem.* 282:26552–26561. https://doi.org/10.1074/jbc.M703158200

Kizhatil, K., S.A. Baker, V.Y. Arshavsky, and V. Bennett. 2009. Ankyrin-G promotes cyclic nucleotide-gated channel transport to rod photoreceptor sensory cilia. *Science.* 323:1614–1617. https://doi.org/10.1126/science.1169789

Kremers, G.J., S.G. Gilbert, P.J. Cranfill, M.W. Davidson, and D.W. Piston. 2011. Fluorescent proteins at a glance. *J. Cell Sci.* 124:157–160. https://doi.org/10.1242/jcs.072744

Lambert, S., J.Q. Davis, and V. Bennett. 1997. Morphogenesis of the node of Ranvier: co-clusters of ankyrin and ankyrin-binding integral proteins

define early developmental intermediates. *J. Neurosci.* 17:7025–7036. https://doi.org/10.1523/JNEUROSCI.17-18-07025.1997

Lasiecka, Z.M., and B. Winckler. 2011. Mechanisms of polarized membrane trafficking in neurons -- focusing in on endosomes. *Mol. Cell. Neurosci.* 48:278–287. https://doi.org/10.1016/j.mcn.2011.06.013

Lois, C., E.J. Hong, S. Pease, E.J. Brown, and D. Baltimore. 2002. Germline transmission and tissue-specific expression of transgenes delivered by lentiviral vectors. *Science.* 295:868–872. https://doi.org/10.1126/science.1067081

Maas, C., V.I. Torres, W.D. Altrock, S. Leal-Ortiz, D. Wagh, R.T. Terry-Lorenzo, A. Fejtova, E.D. Gundelfinger, N.E. Ziv, and C.C. Garner. 2012. Formation of Golgi-derived active zone precursor vesicles. *J. Neurosci.* 32:11095–11108. https://doi.org/10.1523/JNEUROSCI.0195-12.2012

Maday, S., A.E. Twelvetrees, A.J. Moughamian, and E.L. Holzbaur. 2014. Axonal transport: cargo-specific mechanisms of motility and regulation. *Neuron.* 84:292–309. https://doi.org/10.1016/j.neuron.2014.10.019

Maurel, P., S. Einheber, J. Galinska, P. Thaker, I. Lam, M.B. Rubin, S.S. Scherer, Y. Murakami, D.H. Gutmann, and J.L. Salzer. 2007. Nectin-like proteins mediate axon Schwann cell interactions along the internode and are essential for myelination. *J. Cell Biol.* 178:861–874. https://doi.org/10.1083/jcb.200705132

McMahon, H.T., and E. Boucrot. 2011. Molecular mechanism and physiological functions of clathrin-mediated endocytosis. *Nat. Rev. Mol. Cell Biol.* 12:517–533. https://doi.org/10.1038/nrm3151

Nakata, T., S. Terada, and N. Hirokawa. 1998. Visualization of the dynamics of synaptic vesicle and plasma membrane proteins in living axons. *J. Cell Biol.* 140:659–674. https://doi.org/10.1083/jcb.140.3.659

Rasband, M.N., and E. Peles. 2016. The Nodes of Ranvier: Molecular Assembly and Maintenance. *Cold Spring Harb. Perspect. Biol.* 8:a020495. https://doi.org/10.1101/cshperspect.a020495

Salzer, J.L., P.J. Brophy, and E. Peles. 2008. Molecular domains of myelinated axons in the peripheral nervous system. *Glia.* 56:1532–1540. https://doi.org/10.1002/glia.20750

Shcherbo, D., C.S. Murphy, G.V. Ermakova, E.A. Solovieva, T.V. Chepurnykh, A.S. Shcheglov, V.V. Verkhusha, V.Z. Pletnev, K.L. Hazelwood, P.M. Roche, et al. 2009. Far-red fluorescent tags for protein imaging in living tissues. *Biochem. J.* 418:567–574. https://doi.org/10.1042/BJ20081949

Sherman, D.L., S. Tait, S. Melrose, R. Johnson, B. Zonta, F.A. Court, W.B. Macklin, S. Meek, A.J. Smith, D.F. Cottrell, et al. 2005. Neurofascins are required to establish axonal domains for saltatory conduction. *Neuron.* 48:737–742. https://doi.org/10.1016/j.neuron.2005.10.019

Shin, K.J., E.A. Wall, J.R. Zavzavadjian, L.A. Santat, J. Liu, J.I. Hwang, R. Rebres, T. Roach, W. Seaman, M.I. Simon, et al. 2006. A single lentiviral vector platform for microRNA-based conditional RNA interference and coordinated transgene expression. *Proc. Natl. Acad. Sci. USA.* 103:13759–13764. https://doi.org/10.1073/pnas.0606179103

Smith, K.R., K.J. Kopeikina, J.M. Fawcett-Patel, K. Leaderbrand, R. Gao, B. Schürmann, K. Myczek, J. Radulovic, G.T. Swanson, and P. Penzes. 2014. Psychiatric risk factor ANK3/ankyrin-G nanodomains regulate the structure and function of glutamatergic synapses. *Neuron.* 84:399–415. https://doi.org/10.1016/j.neuron.2014.10.010

Snapp, E. 2005. Design and use of fluorescent fusion proteins in cell biology. Curr. Protoc. Cell Biol. 27:21.4.1–21.4.13.

Susuki, K., and M.N. Rasband. 2008. Molecular mechanisms of node of Ranvier formation. *Curr. Opin. Cell Biol.* 20:616–623. https://doi.org/10.1016/j.ceb.2008.09.007

Tan, J.Z.A., and P.A. Gleeson. 2019. Cargo Sorting at the *trans*-Golgi Network for Shunting into Specific Transport Routes: Role of Arf Small G Proteins and Adaptor Complexes. *Cells.* 8:531. https://doi.org/10.3390/cells8060531

Volkmer, H., B. Hassel, J.M. Wolff, R. Frank, and F.G. Rathjen. 1992. Structure of the axonal surface recognition molecule neurofascin and its relationship to a neural subgroup of the immunoglobulin superfamily. *J. Cell Biol.* 118:149–161. https://doi.org/10.1083/jcb.118.1.149

Yap, C.C., M. Vakulenko, K. Kruczek, B. Motamedi, L. Digilio, J.S. Liu, and B. Winckler. 2012. Doublecortin (DCX) mediates endocytosis of neurofascin independently of microtubule binding. *J. Neurosci.* 32:7439–7453. https://doi.org/10.1523/JNEUROSCI.5318-11.2012

Yap, C.C., L. Digilio, K. Kruczek, M. Roszkowska, X.Q. Fu, J.S. Liu, and B. Winckler. 2018. A dominant dendrite phenotype caused by the disease-associated G253D mutation in doublecortin (DCX) is not due to its endocytosis defect. *J. Biol. Chem.* 293:18890–18902. https://doi.org/10.1074/jbc.RA118.004462

Young, J.I., S. Züchner, and G. Wang. 2015. Regulation of the Epigenome by Vitamin C. *Annu. Rev. Nutr.* 35:545–564. https://doi.org/10.1146/annurev-nutr-071714-034228

Zhang, X., and V. Bennett. 1998. Restriction of 480/270-kD ankyrin G to axon proximal segments requires multiple ankyrin G-specific domains. *J. Cell Biol.* 142:1571–1581. https://doi.org/10.1083/jcb.142.6.1571

Zhang, X., J.Q. Davis, S. Carpenter, and V. Bennett. 1998. Structural requirements for association of neurofascin with ankyrin. *J. Biol. Chem.* 273:30785–30794. https://doi.org/10.1074/jbc.273.46.30785

Zhang, Y., Y. Bekku, Y. Dzhashiashvili, S. Armenti, X. Meng, Y. Sasaki, J. Milbrandt, and J.L. Salzer. 2012. Assembly and maintenance of nodes of ranvier rely on distinct sources of proteins and targeting mechanisms. *Neuron.* 73:92–107. https://doi.org/10.1016/j.neuron.2011.10.016

JCB

# Supplemental material

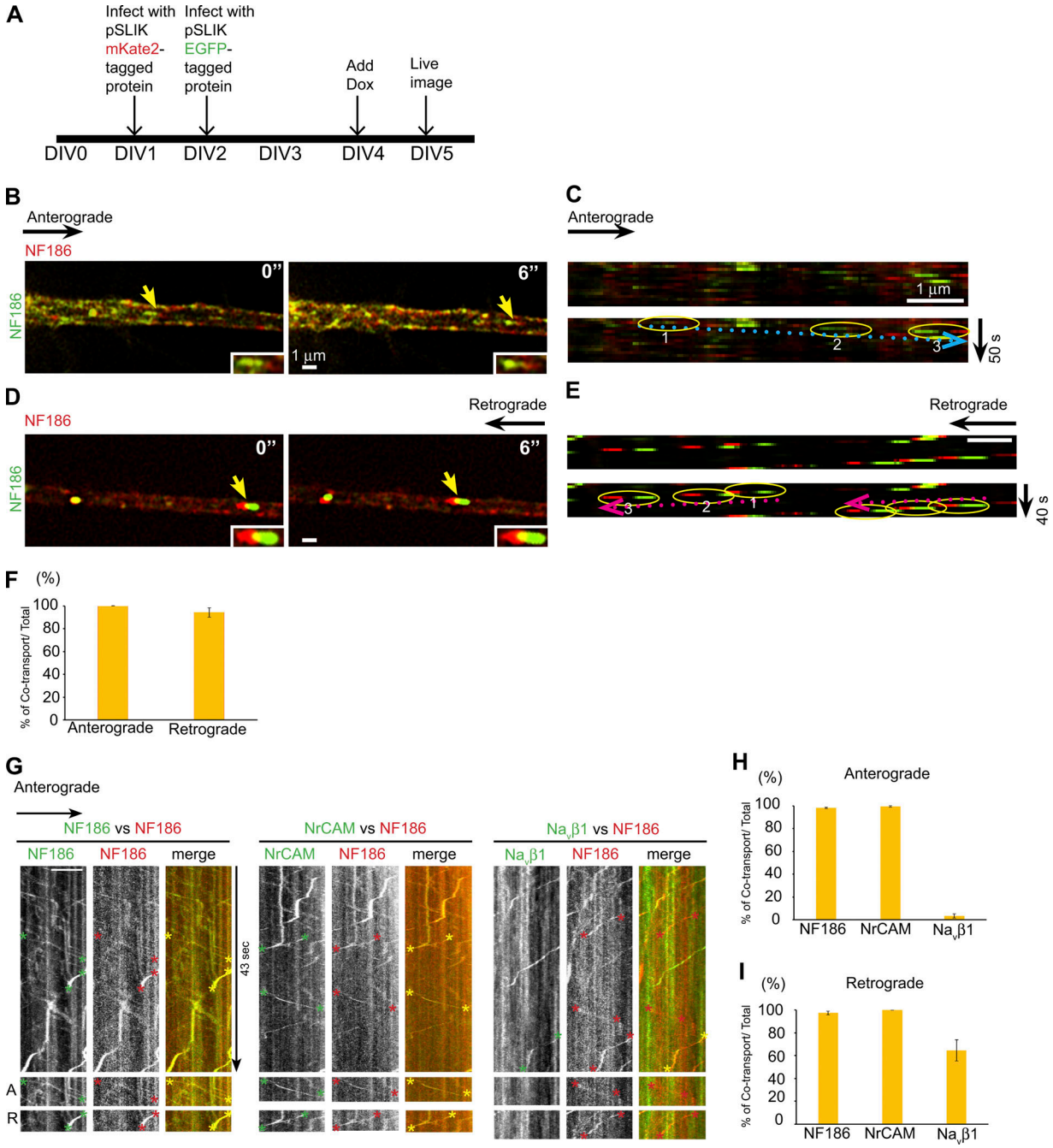


Figure S1. **NF186-EGFP and NF186-mKate2 are uniformly cotransported bidirectionally. (A)** Schematic of the time course and design of the experiment. **(B–E)** NF186-EGFP and NF186-mKate2 are uniformly cotransported bidirectionally. Representative micrographs captured from live imaging and kymographs in the anterograde direction (B and C) and retrograde (D and E) direction. Yellow arrows indicate vesicles cotransporting both cargoes. Trajectories of each vesicle are circled (yellow for cotransport) and numbered in temporal sequence; dotted blue and red arrows indicate anterograde and retrograde directions, respectively. Scale bars, 1 µm. **(F)** The bar graph shows the percentages of vesicles that coexpress mKate2 and EGFP versus the total numbers of mKate2 vesicles; error bars indicate mean ± SEM.. **(G)** Representative kymographs captured by spinning disk microscopy show bidirectional transport of NF186-mKate2 with NF186-EGFP, with NrCAM-EGFP, and with Na$_v$β1-EGFP; both channels were imaged simultaneously. EGFP and mKate2 trajectories are marked by green asterisks and red asterisks, respectively. Cotransport is evident as yellow trajectories in the merged images and indicated by yellow asterisks. Images shown below are specific examples of anterograde (A) and retrograde (R) trajectories. NF186 and Na$_v$β1 exhibit cotransport only in the retrograde direction. **(H)** Quantification of vesicles that colabeled for NF186-mKate2 and the indicated EGFP-positive component versus the total number of anterogradely transported NF186-mKate2 vesicles are shown. NF186 and NrCAM are uniformly cotransported, whereas Na$_v$β1 exhibits negligible cotransport. The corresponding percentages of cotransported vesicles are NF186, 98.2% ± 0.7% ($n$ = 14); NrCAM, 99.4% ± 0.6% ($n$ = 14); and Na$_v$β1, 3.3% ± 1.7% ($n$ = 9); error bars indicate mean ± SEM. **(I)** Quantification of vesicles that colabel for NF186 and the indicated EGFP+ component versus the total number of retrogradely transported NF186-mKate2 vesicles are shown. NF186 is uniformly cotransported with NrCAM and substantially cotransported with Na$_v$β1 as shown. The corresponding percentages of cotransported vesicles are NF186, 97.5% ± 1.5% ($n$ = 14); NrCAM, 100% ($n$ = 14); and Na$_v$β1, 64.7% ± 9.3% ($n$ = 8); error bars indicate mean ± SEM.

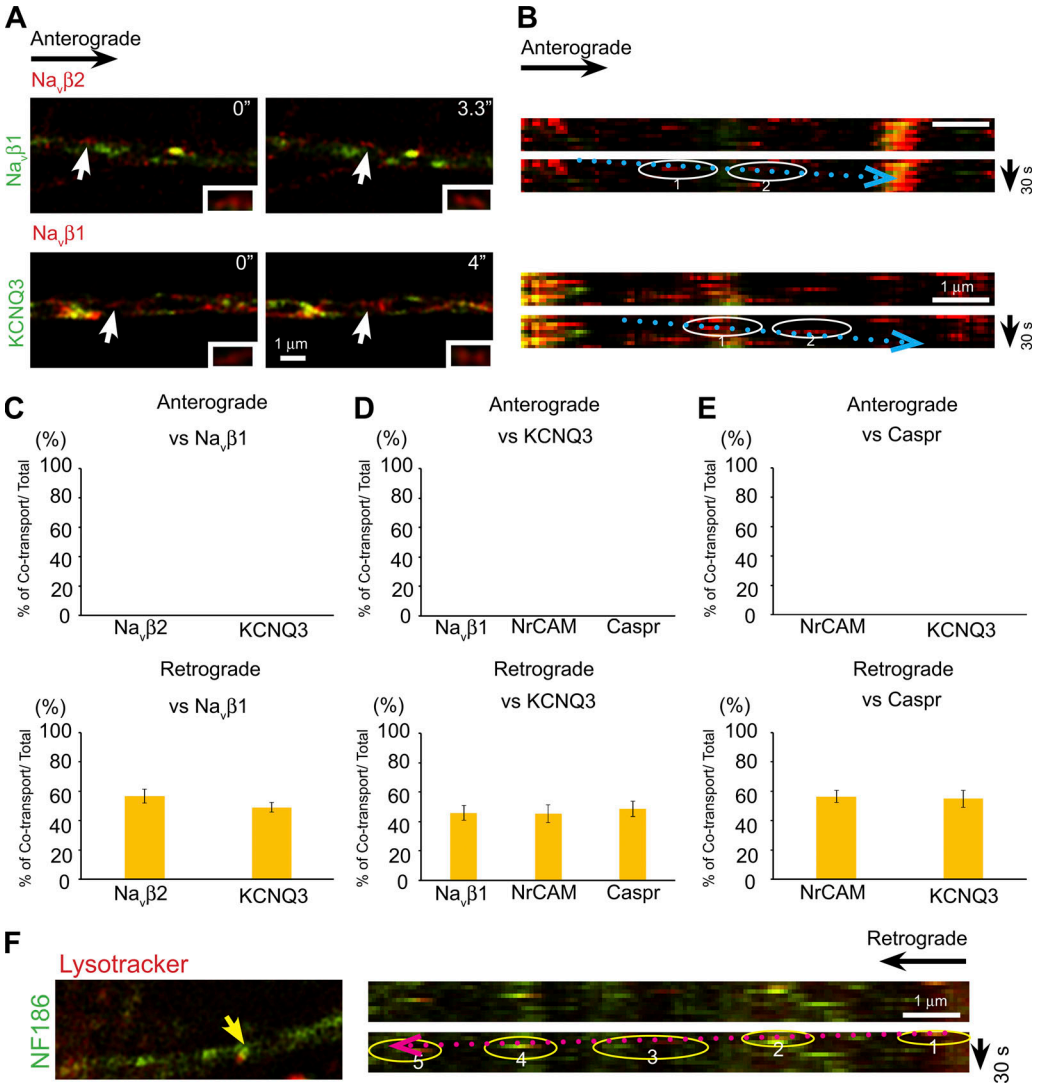


Figure S2. **Other domain components are transported independently in the anterograde direction and substantially cotransported in the retrograde direction**. **(A)** Representative micrographs captured from live images show transport of Na$_v$β2-mKate2 versus Na$_v$β1-EGFP (top row) and Na$_v$β1-mKate2 versus KCNQ3-EGFP (bottom row) in the anterograde direction. White arrows indicate examples of vesicles that are only mKate2 labeled. Insets show higher power images of vesicles indicated by the arrows. Time of imaging (seconds) is indicated in each panel. **(B)** Corresponding duplicate kymographs of anterogradely transported vesicles, indicated by the white arrows in A, are shown circled and their trajectories are indicated by the dotted blue arrows. Scale bars, 1 µm. **(C)** Quantification of cotransport for the constructs indicated. In the anterograde direction (top panel), no cotransport was observed for Na$_v$β2-mKate2 with Na$_v$β1-EGFP (15 axons, 97 vesicles) or KCNQ3-mKate2 with Na$_v$β1-EGFP (15 axons, 96 vesicles). There was substantial cotransport in the retrograde direction (bottom panel) for Na$_v$β2-EGFP with Na$_v$β1-mKate2 (56.8% ± 4.7%, *n* = 15 axons, 144 vesicles) and KCNQ3-EGFP with Na$_v$β1-mKate2 (45.8% ± 5.0%, *n* = 14 axons, 122 vesicles). Error bars indicate mean ± SEM. **(D)** Quantification of cotransport for the constructs indicated. In the anterograde direction (top panel), no cotransport was observed for Na$_v$β1-mKate2 with KCNQ3-EGFP (14 axons, 96 vesicles), for NrCAM-mKate2 with KCNQ3-EGFP (14 axons, 76 vesicles), or for Caspr-EGFP with KCNQ3-mKate2 (21 axons, 96 vesicles). In the retrograde direction (bottom panel), there was substantial cotransport for Na$_v$β2-mKate2 with Na$_v$β1-EGFP (56.8% ± 4.7%, *n* = 15 axons, 144 vesicles), for KCNQ3-EGFP with Na$_v$β1-mKate2 (45.8% ± 5.0%, *n* = 14 axons, 122 vesicles), and for Caspr-EGFP with KCNQ3-mKate2 (48.6% ± 5.1%, *n* = 21 axons, 166 vesicles). Error bars indicate mean ± SEM. **(E)** Quantification of cotransport for the constructs indicated. In the anterograde direction (top panel), no cotransport was observed for NrCAM-mKate2 with Caspr-EGFP (15 axons, 72 vesicles) or for KCNQ3-mKate2 with Caspr-EGFP (21 axons, 96 vesicles). In the retrograde direction (bottom panel), there was substantial cotransport for NrCAM-mKate2 with Caspr-EGFP (49.2% ± 4.2%, *n* = 15 axons, 118 vesicles) and for KCNQ3-mKate2 with Caspr-EGFP (54.8% ± 5.7%, *n* = 21 axons, 166 vesicles). Error bars indicate mean ± SEM. **(F)** An example of NF186-EGFP–containing vesicle that colabeled with Lysotracker is indicated by the yellow arrow in the micrograph (left) and circled in the kymograph (right); its retrograde trajectory is indicated by the dotted red arrow. Axon numbers analyzed: *n* = 10.

Video 1. **Examples of vesicle transport of NF186 and $Na_v\beta2$**. Video showing $Na_v\beta2$-EGFP is transported by tubular-like vesicles in the anterograde direction (indicated by green arrowheads at t = 0 and t = 1 min); images were captured at 2.5-s time intervals. NF186-mKate2 and $Na_v\beta2$-EGFP are cotransported by a vesicle (yellow arrowhead) actively moving in the retrograde direction. Green and red fluorescence from the same vesicles intermittently appear to diverge due to the sequential capture of green and red fluorescence channels on our microscope; the faster the vesicle is moving at the time of acquisition, the larger the apparent displacement between green and red fluorescence.

Video 2. **Examples of vesicle transport of NF186 and Caspr.** Video of the retrograde transport of NF186-mKate2 and Caspr-EGFP; two vesicles are shown. One contains both NF186-mKate2 and Caspr-EGFP (yellow arrowhead); the red and green images diverge during active transport and then largely overlap when this vesicle is stationary. The other vesicle only contains Caspr (indicated by the green arrowhead beginning at t = 11 s). Images were captured at 3.5-s time intervals.

**Table S1 is provided online and lists the transport velocities of vesicles containing various axonal proteins.**